




Upconversion luminescence and time decay study of Yb–Er-doped BaWO₄ nanophosphor

Arnab De⁴, Arnab Kumar Dey^{4,1}, Bibek Samanta^{4,2}, Soumyadeep Sur^{4,3}, Sourav Paul^{4,6}, Ashadul Adalder^{4,6}, Swati Das^{6,*}, and Uttam Kumar Ghorai^{4,5,*} 

¹ Present address: Department of Materials Science and Engineering, IIT Delhi, Delhi 110016, India

² Present address: Department of Metallurgical Engineering & Materials Science, IIT Bombay, Mumbai 400076, India

³ Present address: Department of Materials Science, Sardar Patel University, Anand 388120, India

⁴ Department of Industrial & Applied Chemistry, Swami Vivekananda Research Centre, Ramakrishna Mission Vidyamandira, Belur Math, Howrah 711202, India

⁵ School of Physical Sciences, Indian Association for the Cultivation of Science, Jadavpur, Kolkata 700032, India

⁶ Department of Physics, Ananda Mohan College, Kolkata 700009, India

Received: 30 June 2021

Accepted: 14 December 2021

Published online:

4 February 2022

© The Author(s), under exclusive licence to Springer Science+Business Media, LLC, part of Springer Nature 2022

ABSTRACT

Rare earth-doped phosphor materials have always remained in focus for excellent luminescence properties. Herein we have synthesized Yb³⁺ and Er³⁺-doped BaWO₄ nanophosphor via facile hydrothermal method with red and green region emissions by 980 nm excitation. Red and green region emissions were observed due to ⁴F_{9/2} → ⁴I_{15/2} and ²H_{11/2}/⁴S_{3/2} → ⁴I_{15/2} transitions, respectively, of Er³⁺, where Yb³⁺ acts as a sensitizer. The sample characterization was done using X-Ray Diffraction (XRD), Fourier Transform Infrared Spectroscopy (FTIR), Transmission Electron Microscopy (TEM), and X-ray Photoelectron Spectroscopy (XPS) techniques. The consequences of different concentrations of activator ion (Er³⁺) in BaWO₄: Yb³⁺, Er³⁺ were studied from luminescence perspective in detail. The intensity of overall emission varied with altering the power of excitation that influences the photon transfer pathways. It was found that two-photon processes control both red and green emissions in the upconversion process. Decay behavior for both the emission was investigated. Thus, the tunable photoluminescence property suggests its potential in optoelectronic applications.

1 Introduction

Research on trivalent lanthanide-doped upconversion (UC) phosphor materials have attracted broad attention during the past decade for their widespread

application in diverse areas, like solid-state lighting [1], solar cells [2–4], temperature sensors [5], anti-counterfeiting security inks [6–9], modern display devices [10], and biomedical imaging [11–13]. The lanthanides show characteristic visible emissions

Address correspondence to E-mail: swati.nanosc@gmail.com; uttamindchem00@gmail.com

because well-shielded 4f electrons show sharp intra-4f transitions [14, 15]. An important criterion of obtaining efficient phosphor lies in careful selection of the host compound. UC luminescence intensity is greatly enhanced by host materials having lower phonon energy as they decrease non-radiative energy transfers [10]. Among numerous inorganic materials, tungstates have drawn significant attraction due to their easy synthesis method [16, 17], chemical stability [18], yield and lower phonon energy [19]. Compared to the sol-gel and co-precipitation method, hydrothermal synthesis uses water as the reaction medium. The synthesis cost is low and reaction conditions are more controllable which cause advantages of producing crystal of better purity and uniform dispersion [8]. For UC phosphors, Yb^{3+} ion (sensitizer) has large absorption around the commonly used 980 nm excitation source [20, 21]. Yb^{3+} ions transfer the absorbed radiation to activator ions and the activators show different characteristic emissions from their step-like energy levels. Among various rare earth elements, Er^{3+} ion is well known due to its characteristic green (${}^2\text{H}_{11/2}/{}^4\text{S}_{3/2} \rightarrow {}^4\text{I}_{15/2}$) and red (${}^4\text{F}_{9/2} \rightarrow {}^4\text{I}_{15/2}$) emission [22–25]. These emissions are utilized to prepare phosphors with visible emissions [26, 27].

Herein, we have explored the consequences of varying Er^{3+} concentrations on UC luminescence properties of Yb, Er codoped BaWO_4 synthesized via hydrothermal method. XRD, FTIR, TEM, and XPS studies were done for structural characterization.

2 Experimental

For BaWO_4 : Yb^{3+} , Er^{3+} phosphor synthesis, barium nitrate [$(\text{Ba}(\text{NO}_3)_2)$ (purity 99.99%, Merck)], sodium tungstate [$(\text{Na}_2\text{WO}_4 \cdot 2\text{H}_2\text{O})$ (purity 99.99%, Merck)], ytterbium oxide [(Yb_2O_3) (purity 99.99%, Merck)], and erbium oxide [(Er_2O_3) (purity 99.99%, Merck)] were taken as precursors. Amounts of the cations were as follows: $(1-x-y)\text{Ba}^{2+}$: $x\text{Yb}^{3+}$: $y\text{Er}^{3+}$, where $x = 0.05$ and $y = 0.01, 0.02, 0.03,$ and 0.04 . Firstly, Yb_2O_3 and Er_2O_3 were separately taken into small quantity of dilute nitric acid followed by simultaneous heating and stirring. $\text{Ba}(\text{NO}_3)_2$ and $\text{Na}_2\text{WO}_4 \cdot 2\text{H}_2\text{O}$ were added into deionized water in a beaker. This aqueous solution was heated and stirred simultaneously (~ 30 min) until the solution changed into white flocculent liquid. Next, the well

dissolved rare earth solutions prepared initially were mixed thoroughly with the white flocculent liquid by 30 min of stirring and pH was raised to 9 by careful addition of ammonium hydroxide solution. The solution was then sealed in Teflon-lined stainless steel autoclave and put at 190 °C for 18 h followed by natural cooling to ambient temperature. Washing of the precipitate was done with ethanol and deionized water for impurity removal and dried for ~ 12 h at 80 °C.

3 Characterization

The crystal structure determination was done using Bruker D8 ADVANCE ECO diffractometer with monochromatic Cu K_α radiation ($\lambda = 1.5406 \text{ \AA}$). The tube current and voltage during the experiment were 25 mA and 40 kV, respectively. The microscopic images of nanophosphors were taken by JEOL TEM (FEG-TEM, JEOL-JEM 2100F). FTIR characterization was performed by Shimadzu IRAffinity-1S. XPS measurement was recorded using OMICRON X-ray photoelectron spectrometer (serial number: 0571) with Al K_α X-ray source. Photoluminescence (PL) property was investigated by Edinburgh FLS 980 Photoluminescence Spectrometer with a 980 nm excitation source. Chromaticity coordinates were calculated using the 1931 CIE chromaticity theory.

4 Results and discussion

4.1 Structural analysis

The XRD graphs of BaWO_4 : Yb, Er is represented in Fig. 1a. The diffraction patterns of both pure and doped samples have shown well-matched peaks with standard JCPDS data card number 85–0588, which belongs to tetragonal scheelite-like BaWO_4 with space group $I4_1/a$ [28, 29]. Due to the small size difference of Yb^{3+} and Er^{3+} with the Ba^{2+} ions, all the dopant elements are expected to reside in the Ba^{2+} sites in BaWO_4 (Fig. 1c) [30]. This is evident from the diffraction patterns, where no extra peak corresponding to dopant ions is present. The diffraction patterns suggest effective incorporation of dopants up to the concentration of 5% Yb^{3+} and 4% Er^{3+} without any significant effect on the host crystal structure.

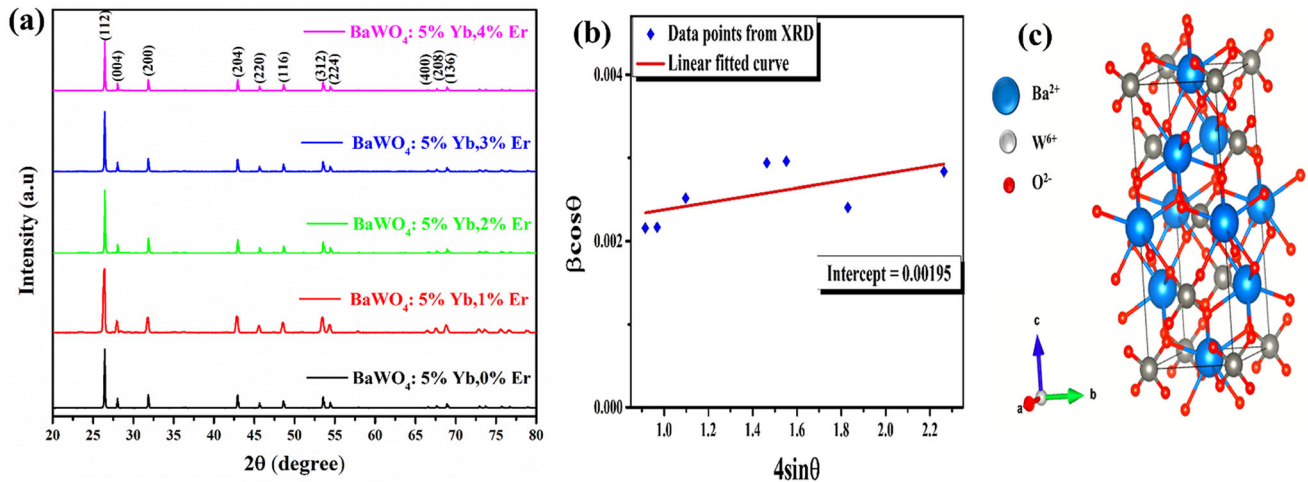


Fig. 1 a XRD patterns of BaWO₄: Yb, Er. b Williamson–Hall plot of BaWO₄: 5%Yb, 3%Er. c Schematic crystal structure of BaWO₄

The Williamson–Hall (W–H) plot is used to calculate the crystallite size and the micro-strain present in the materials. The W–H equation can be given by

$$\beta \cos \theta = 4 \varepsilon \sin \theta + \frac{K\lambda}{D} \quad (1)$$

where β signifies the FWHM measured for different XRD lines corresponding to different planes, ε is the micro-strain inside the material, and D is the crystallite size. The exact value of K is not known for the present materials system, hence $K = 1$ was used and D value obtained from the intercept are only estimates. Equation 1 represents a straight line between $4\sin\theta$ (X-axis) and $\beta\cos\theta$ (Y-axis). The slope of the line gives the strain (ε) and the intercept (λ/D) of this line on the Y-axis gives grain size (D) [29]. From the intercept of W–H plot, crystallite size was found to be around 79 nm (Fig. 1b).

Particle morphology and size of synthesized phosphors are illustrated in Fig. 2. Distorted spherical-type particles with size ~ 50 – 100 nm were found for BaWO₄: Yb, Er as indicated in Fig. 2a. The lattice image of the nanophosphor showing different arrays of atoms is presented in Fig. 2b.

Figure 3 shows the FTIR spectra of pure BaWO₄ and BaWO₄: Yb, Er. The sharp absorption peak observed around 800 cm^{-1} is attributed to the anti-symmetric stretching of the W–O bonds present in WO₄²⁻ groups [29]. Small peak near 1500 cm^{-1} is due to carboxylate groups coming from citrate ions used during synthesis.

XPS is a useful surface characterization technique to confirm presence of dopant elements in the host

material. XPS data taken for BaWO₄: 5% Yb, 3% Er sample are presented in Fig. 4. The survey spectrum (Fig. 4a) confirms the presence of Ba, W, O, Yb, and Er in the sample. High-resolution spectrum of Ba 3d (Fig. 4b) reveals two peaks at 778.7 and 794.1 eV corresponding to Ba 3d_{5/2} and Ba 3d_{3/2}, respectively. For W 4f (Fig. 4c) there are two peaks at 34.2 and 36.4 eV due to W 4f_{7/2} and W 4f_{5/2}, respectively. Peak fitting for Yb 4d leads to identification of four main peaks in the range of 174–202 eV (Fig. 4d). Fitting for Er 4d shows a peak at 168 eV (Fig. 4e). All the peaks are in well accordance with previously reported data [31].

4.2 Photoluminescence study

As shown in Fig. 5a, emission peaks were observed in the regions of 515–575 nm and 625–685 nm for BaWO₄: Yb, Er. For constant Yb³⁺ concentration of 5 mol %, Er³⁺ was taken from 1 mol% to 4 mol%. As shown in Fig. 5, the emission intensity gradually increases from 1 mol% up to 3 mol% and decreases at 4 mol% of Er³⁺. With increasing Er³⁺ concentration from 1 mol% to 4 mol% and invariable Yb³⁺ concentration (5 mol%), the variation tendency of UC intensities is presented in Fig. 5a and b. The optimum dopant concentration was found to be 5 mol% Yb³⁺ and 3 mol% Er³⁺ for the BaWO₄: Yb, Er phosphors.

If luminescence quenching is due to the energy transfer among identical lanthanide ions, the determination of critical distance (R_c) can be done by the Blasse equation (Eq. 2) [29]

Fig. 2 a TEM micrographs of BaWO₄: 5%Yb, 3%Er. b Lattice image of the nanophosphor

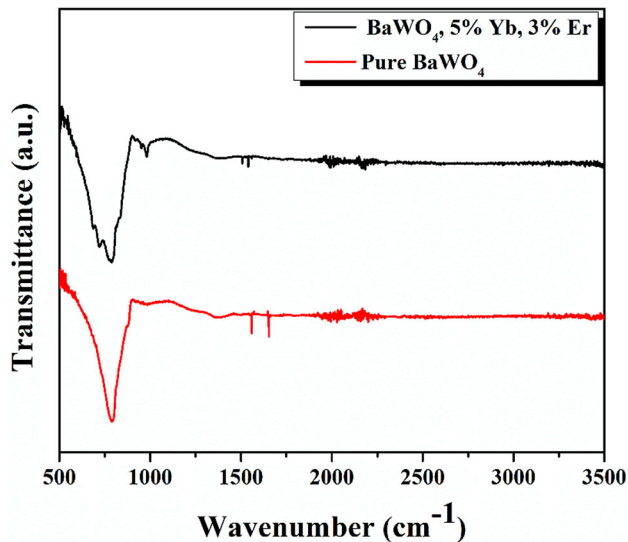
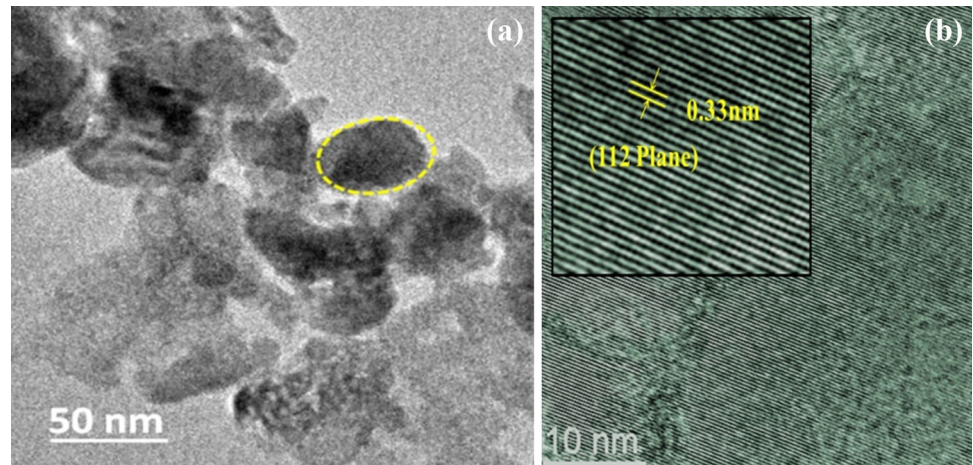


Fig. 3 FTIR spectra of BaWO₄: 5%Yb, 3%Er and pure BaWO₄

$$R_c = 2 \left(\frac{3V}{4\pi X_c N} \right)^{1/3} \quad (2)$$

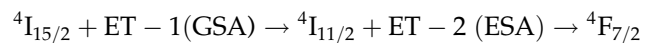
where 'V' = unit cell volume, 'X_c' = activator ion's mole fraction beyond which quenching occurs (critical concentration) and 'N' = crystallographic sites possessed by Er³⁺ in unit cell. For optimized 3 mol% Er³⁺ (X_c = 0.03)-doped phosphors tetragonal system, a = b = 5.613 Å, c = 12.72 Å, Z = 4, V = abc = 400.75 Å³, and N = Z, R_c is calculated to be 18.54 Å. Since R_c is greater than 5 Å, it is concluded that exchange interaction among Er³⁺ ions is not the reason behind concentration quenching, but rather multipolar interaction is involved in it [29, 32].

Chromaticity coordinates calculated using the 1931 CIE chromaticity theory are shown in Fig. 6. CIE

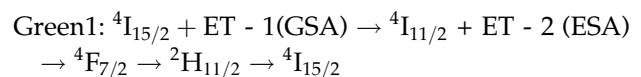
coordinates of different phosphors are tabulated in Table 1.

4.2.1 Photoluminescence mechanism

The UC photoluminescence mechanism consists of different processes, like ground-state absorption (GSA), excited-state absorption (ESA), energy transfer (ET), and non-radiative transfer (NRT). Upon excitation with 980 nm laser, energy was mostly absorbed by the sensitizer Yb³⁺ as Yb³⁺ (~ 11.7 × 10⁻²¹ cm²) has almost 7 times higher absorption cross-section area than Er³⁺ (~ 1.7 × 10⁻²¹ cm²) around 980 nm [33]. This GSA process causes the transition from ground level ²F_{7/2} to the excited level ²F_{5/2} in Yb³⁺. While returning to ground level, the Yb³⁺ ions transfer their energy via different ET processes to the Er³⁺ ions from where further processes for luminescence take place as presented in Fig. 7. For green emissions, two sequential ET processes populate the ⁴F_{7/2} excited state from ground ⁴I_{15/2} as presented below:



Two different non-radiative energy transfers from the excited ⁴F_{7/2} level populate the ²H_{11/2} and ⁴S_{3/2} levels. Subsequent relaxation to ⁴I_{15/2} level gives rise to two green emission bands, i.e., green1 (527 nm) and green2 (541 nm) due to the transitions ²H_{11/2} → ⁴I_{15/2} and ⁴S_{3/2} → ⁴I_{15/2}, respectively.



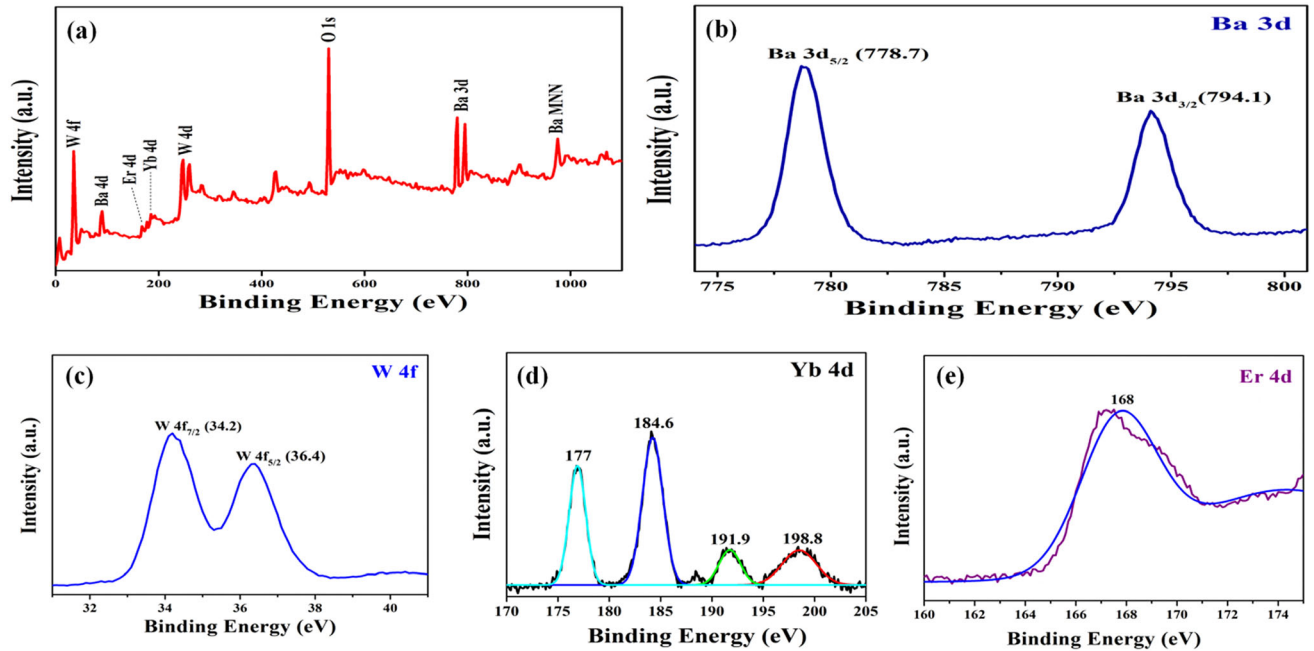


Fig. 4 XPS spectrum of a BaWO₄: 5% Yb, 3% Er and high-resolution spectra of b Ba 3d, c W 4f, d Yb 4d, and e Er 4d

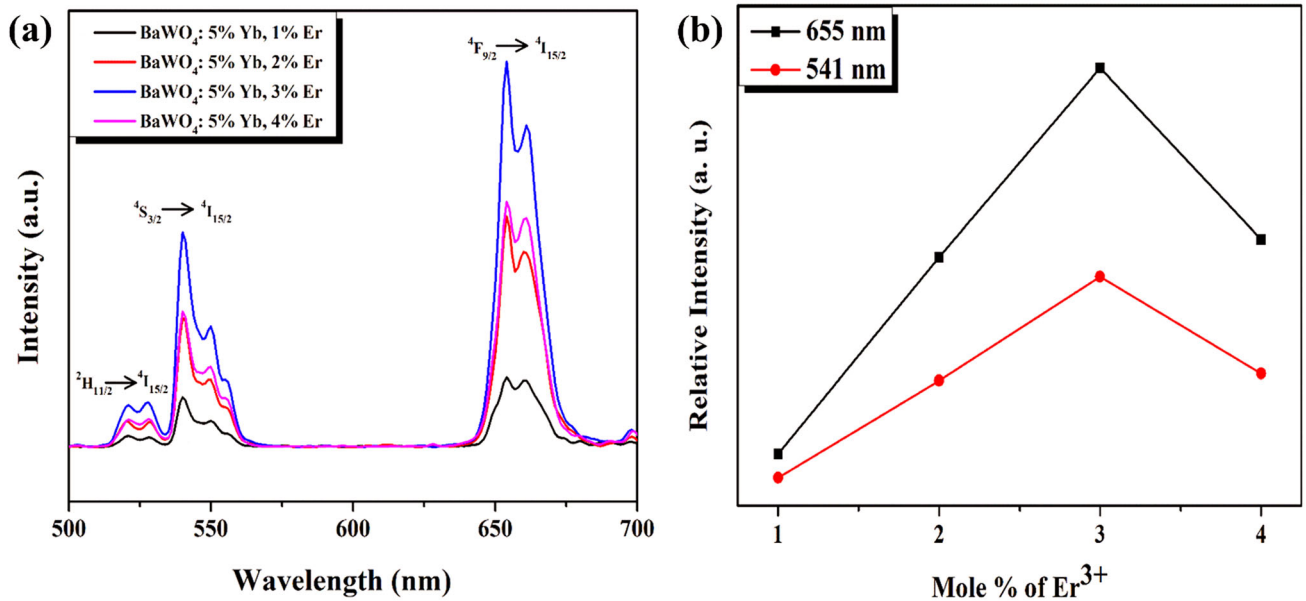
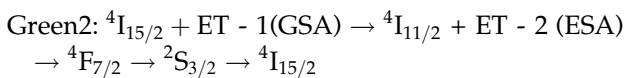
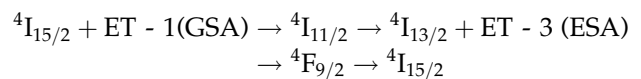


Fig. 5 a PL emission spectra of BaWO₄: Yb, Er. b Relative intensities of the 655 nm and 541 nm emissions for different Er³⁺ concentrations



For red emission, electrons from the excited ${}^4I_{11/2}$ state populate the ${}^4I_{13/2}$ state via an NRT process. An ESA from this ${}^4I_{13/2}$ state populate the ${}^4F_{9/2}$ state. Relaxation from this excited ${}^4F_{9/2}$ level to ground

${}^4I_{15/2}$ level is accompanied by red emission between 640 and 690 nm. Whole process is outlined below:



Relation between pump power (P) of laser source and UC emission intensity (I_{em}) is given by: $I_{em} \propto P^n$,

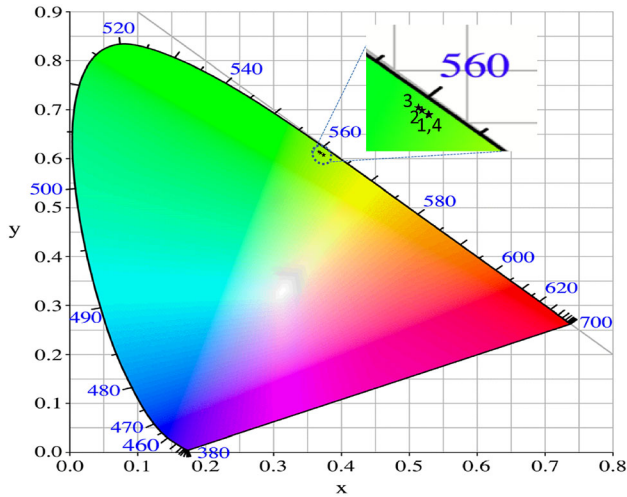


Fig. 6 CIE diagram of BaWO₄: 5% Yb, x% Er, x = 1, 2, 3, 4 (in inset 1, 2, 3, 4 are representing the mole % of Er³⁺)

Table 1 CIE coordinates of BaWO₄: Yb, Er phosphors

Sl. No	Phosphor	x coordinate	y coordinate
1	BaWO ₄ : 5% Yb, 1% Er	0.37375	0.61239
2	BaWO ₄ : 5% Yb, 2% Er	0.36944	0.61619
3	BaWO ₄ : 5% Yb, 3% Er	0.36704	0.61867
4	BaWO ₄ : 5% Yb, 4% Er	0.37434	0.61189

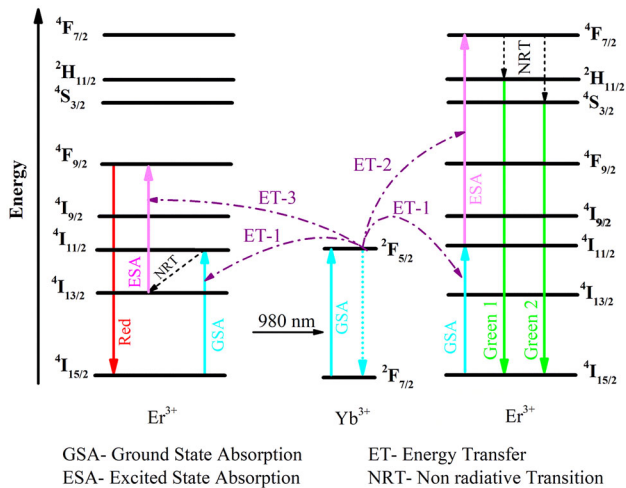


Fig. 7 Schematic representation of energy levels in Yb³⁺ and Er³⁺ along with proposed mechanism for green and red emissions (Color figure online)

where ‘n’ represents the number of photons involved for a particular emission [27]. Value of ‘n’ is found from slope by plotting logarithm of pump power vs logarithm of emitted intensity (lnP vs lnI_{em} graph in

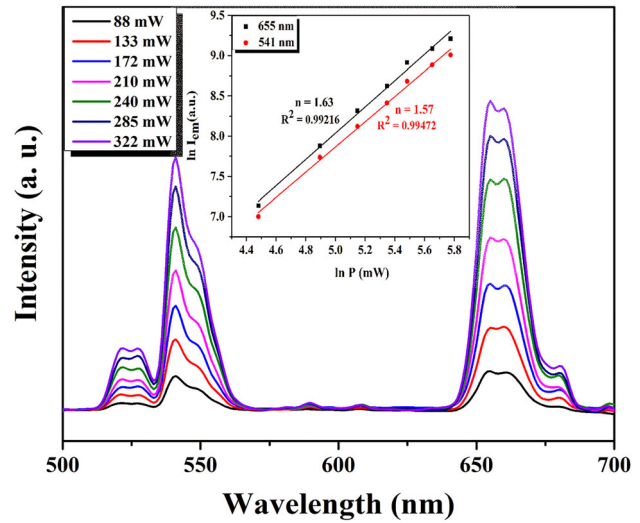


Fig. 8 UC emission intensity with varying pump powers for the BaWO₄: 5%Yb³⁺, 3%Er³⁺. Inset figure shows lnP vs lnI_{em} plot with linear fitting

Fig. 8 inset). The values of ‘n’ measured by curve fitting for 655 nm and 541 nm are 1.63 and 1.57, respectively. The slopes for both emissions prove two-photon processes occur both in 655 nm and 541 nm UC emissions. The values of n obtained are lower than the theoretical value of 2, which indicates the saturation of the upconversion process [1].

To further explore the mechanism, the decay curves of red ⁴F_{9/2} → ⁴I_{15/2} (655 nm) and green ⁴S_{3/2} → ⁴I_{15/2} (541 nm) in BaWO₄: 5%Yb³⁺, 3%Er³⁺ were recorded under pulsed laser excitation of 980 nm.

Figure 9 shows the decay curves of 655 nm and 541 nm emissions of the nanophosphor that were fitted into a mono-exponential and bi-exponential function, respectively, which is in well accordance with the available literature [23]. The bi-exponential decay indicates that more than one decay channel (both radiative and non-radiative) is involved in the total decay process, whereas mono-exponential decay indicate only one kind (radiative) of luminescent center dominates the PL emission. The bi-exponential decay equation (Eq. 3) and the mono-exponential decay equation (Eq. 4) are given below:

$$I(t) = A_1 \exp\left(-\frac{t}{\tau_1}\right) + A_2 \exp\left(-\frac{t}{\tau_2}\right) \tag{3}$$

$$I(t) = I_0 + A_1 \exp\left(-\frac{t}{\tau}\right) \tag{4}$$

where I₀ is the initial luminescence intensity, τ₁ and τ₂ represent fast and slow luminescence lifetime,

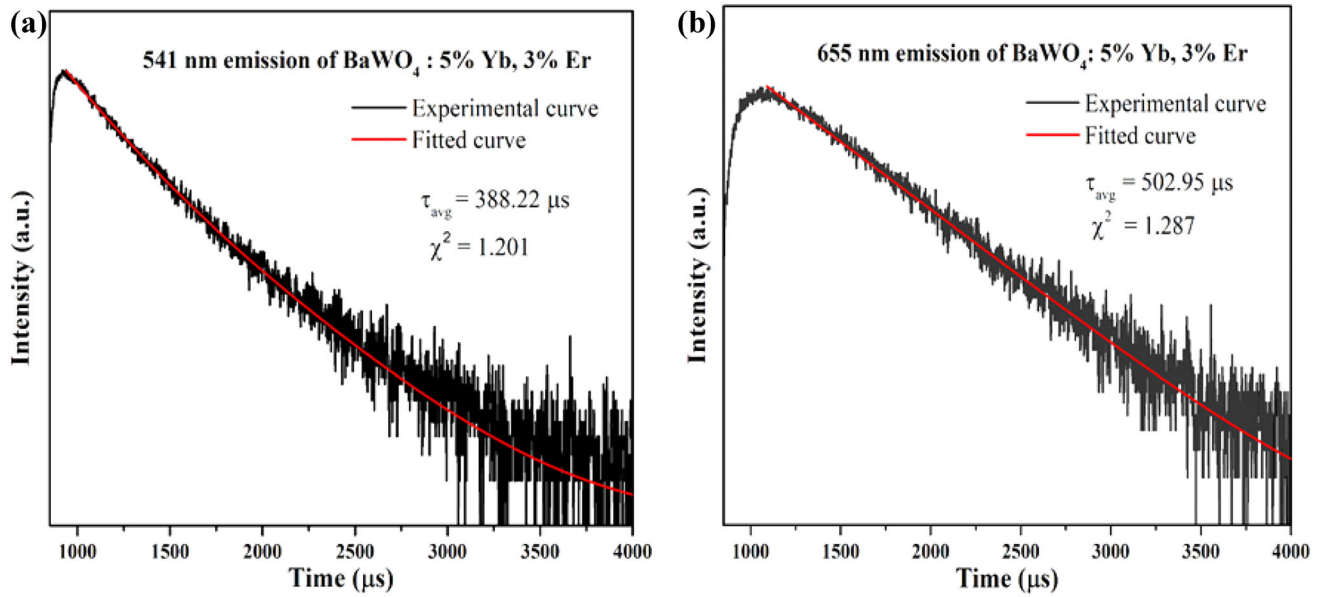


Fig. 9 Time decay curve of BaWO₄: 5% Yb³⁺, 3% Er³⁺ for **a** 541 nm and **b** 655 nm

Table 2 The experimental values of the parameters τ_1 , τ_2 , A_1 , A_2 , and τ_{avg}

	τ_1 (μ s)	τ_2 (μ s)	A_1	A_2	Lifetime (μ s)
655 nm	502.95	–	100	–	$\tau = 502.95$
541 nm	241.2	462.2	48.82	51.18	$\tau_{avg} = 388.22$

respectively, and A_1 and A_2 are the constants (Table 2) [23, 34]. The average lifetime for bi-exponential decay curve is calculated using the equation below (Eq. 5).

$$\tau_{avg} = \frac{A_1\tau_1^2 + A_2\tau_2^2}{A_1\tau_1 + A_2\tau_2} \tag{5}$$

The average lifetime for 541 nm emission was calculated using Eq. 5 and observed lifetime of 655 nm (red) emission and 541 nm (green) emissions was 502.95 μ s and 388.22 μ s, respectively.

5 Conclusion

We have reported BaWO₄: Yb, Er nanophosphor prepared via hydrothermal route. The phosphors have shown green and red emissions corresponding to the transitions ²H_{11/2}/⁴S_{3/2} → ⁴I_{15/2} and ⁴F_{9/2} → ⁴I_{15/2} of Er³⁺, respectively. The concentration of Er³⁺ was optimized to be 3 mol % for the highest luminescence intensity. It was determined that two-

photon processes control both red and green emissions. The average decay time was detected to be in the microsecond region. Overall PL mechanism was discussed accordingly. The results signify that the discussed phosphor may be a suitable option for UC-based lighting applications.

Acknowledgements

UKG acknowledges the Teachers Associateship for Research Excellence (TARE) fellowship and research grant (TAR/2018/000763) of SERB, Govt. of India and thanks the TARE project mentor Prof. A. J. Pal, IACS-Kolkata. UKG acknowledges the central DST-FIST program (SR/FST/College-287/2015) for financial support. UKG thanks the DBT Star College Scheme (BT/HRD/11/036/2019) for funding. UKG also acknowledges Science & Technology and Biotechnology Department, Govt. of West Bengal for providing the financial support [199 (Sanc.)/ST/P/S&T/6G-12/2018]. SD acknowledges the SERB for providing financial support (EEQ/2019/000401). SP gratefully thank SERB, Govt. of India for providing the junior research fellowship (JRF). SD and UKG wish to thank Science & Technology and Biotechnology Department, Govt. of West Bengal for providing the financial support (ST/P/S&T/6G-6/2019). AA thanks Science & Technology and Biotechnology Department, Govt. of West Bengal for JRF.

Author contribution

AD, AKD, BS, and SS synthesized the phosphors and performed the XRD and FTIR characterization. AD, AKD, SP, and AA performed the photoluminescence study. SP and AA analyzed the XPS and HRTEM results. All authors contributed to write the manuscript. SD and UKG supervised the project.

Declarations

Conflict of interest The authors declare that they have no conflicts of interest.

Human and animal consent This article does not contain any studies with human participants or animals performed by any of the authors.

References

1. V. Mahalingam, R. Naccache, F. Vetrone, J.A. Capobianco, Enhancing upconverted white light in $\text{Tm}^{3+}/\text{Yb}^{3+}/\text{Ho}^{3+}$ -doped GdVO_4 nanocrystals via incorporation of Li^+ ions. *Opt. Express*. **20**, 111–119 (2012). <https://doi.org/10.1364/OE.20.000111>
2. D.R. Kim, S.W. Park, B.K. Moon, S.H. Park, J.H. Jeong, H. Choi, J.H. Kim, The role of Yb^{3+} concentrations on Er^{3+} doped SrLaMgTaO_6 double perovskite phosphors. *RSC Adv*. **7**, 1464–1470 (2017). <https://doi.org/10.1039/C6RA24808J>
3. P. Kumar, B.K. Gupta, New insight into rare-earth doped gadolinium molybdate nanophosphor assisted broad spectral converter from UV to NIR for silicon solar cell. *RSC Adv*. **5**, 24729–24736 (2015). <https://doi.org/10.1039/C4RA15383A>
4. T. Li, C.F. Guo, Y.M. Yang, L. Li, N. Zhang, Efficient green up-conversion emission in $\text{Yb}^{3+}/\text{Ho}^{3+}$ co-doped CaIn_2O_4 . *Acta Mater*. **61**, 7481–7487 (2013). <https://doi.org/10.1016/j.actamat.2013.08.060>
5. O.A. Savchuk, J.J. Carvajal, M.C. Pujol, E.W. Barrera, J. Massons, M. Aguilo, F. Diaz, Ho, Yb:KLu(W_{O_4})₂ nanoparticles: A versatile material for multiple thermal sensing purposes by luminescent thermometry. *J. Phys. Chem. C* **119**, 18546–18558 (2015). <https://doi.org/10.1021/acs.jpcc.5b03766>
6. P. Kanika, S. Kumar, B.K.G. Singh, A novel approach to synthesis a dual mode luminescent composite pigment for uncloneable high security codes to combat counterfeiting. *Chem. A Eur. J*. **23**, 17144–17151 (2017). <https://doi.org/10.1002/chem.201704076>
7. P. Kumar, J. Dwivedi, B.K. Gupta, Highly-luminescent dual mode rare-earth nanorods assisted multi-stage excitable security ink for anti-counterfeiting applications. *J. Mater. Chem. C* **2**, 10468–10475 (2014). <https://doi.org/10.1039/C4TC02065K>
8. P. Kumar, S. Singh, B.K. Gupta, Future prospects of luminescent nanomaterials based security ink: From synthesis to anti-counterfeiting applications. *Nanoscale* **8**, 14297–14340 (2016). <https://doi.org/10.1039/C5NR06965C>
9. P. Kumar, K. Nagpal, B.K. Gupta, Unclonable security codes designed from multicolour luminescent lanthanide-doped Y_2O_3 nanorods for anticounterfeiting. *ACS Appl. Mater. Interfaces* **9**, 14301–14308 (2017). <https://doi.org/10.1021/aciamsi.7b03353>
10. F. Li, L. Li, C. Guo, T. Li, H. Mi, J.H. Jeong, Up-conversion luminescence properties of Yb^{3+} – Ho^{3+} co-doped $\text{CaLa}_2\text{-ZnO}_5$. *Ceram. Int*. **40**, 7363–7366 (2014). <https://doi.org/10.1016/j.ceramint.2013.12.080>
11. B. Liu, C. Li, Z. Xie, Z. Hou, Z. Cheng, D. Jin, J. Lin, 808 nm photocontrolled UCL imaging guided chemo/photothermal synergistic therapy with single UCNPs-CuS@PAA nanocomposite. *Dalton Trans*. **45**, 13061–13069 (2016). <https://doi.org/10.1039/C5DT04857E>
12. Z. Zhang, J. Sheng, M. Zhang, X. Ma, Z. Geng, Z. Wang, Dual-modal imaging and excellent anticancer efficiency of cisplatin and doxorubicin loaded $\text{NaGdF}_4:\text{Yb}^{3+}/\text{Er}^{3+}$ nanoparticles. *RSC Adv*. **8**, 22216–22225 (2018). <https://doi.org/10.1039/C8RA03898H>
13. C. Li, D. Yang, P. Ma, Y. Chen, Y. Wu, Z. Hou, Y. Dai, J. Zhao, C. Sui, J. Lin, Multifunctional upconversion mesoporous silica nanostructures for dual modal imaging and in vivo drug delivery. *Small* **90**, 4150–4159 (2013). <https://doi.org/10.1002/sml.201301093>
14. R. Chatterjee, S. Saha, D. Sen, K. Panigrahi, U.K. Ghorai, G.C. Das, K.K. Chattopadhyay, Neutralizing the charge imbalance problem in Eu^{3+} -activated BaAl_2O_4 nanophosphors: Theoretical insights and experimental validation considering K^+ codoping. *ACS Omega* **3**, 788–800 (2018). <https://doi.org/10.1021/acsomega.7b01525>
15. A. De, A.K. Dey, B. Samanta, U.K. Ghorai, Enhanced red photoluminescence in chain-like $\text{SrAl}_2\text{O}_4:\text{Eu}^{3+}$ nanophosphors: utilizing charge compensation by modulating Na^+ codoping concentration. *J Mater Sci: Mater Electron* **32**, 8648–8656 (2021). <https://doi.org/10.1007/s10854-021-05524-2>
16. H. Wu, J. Yang, X. Wang, S. Gan, L. Li, Solvent directed morphologies and enhanced luminescent properties of $\text{BaWO}_4:\text{Tm}^{3+}, \text{Dy}^{3+}$ for white light emitting diodes. *Solid State Sci*. **79**, 85–92 (2018). <https://doi.org/10.1016/j.solidstasci.2018.02.009>
17. H.L. Li, Z.L. Wang, S.J. Xu, J.H. Hao, Improved performance of spherical $\text{BaWO}_4:\text{Tb}^{3+}$ phosphors for field-emission

- displays. *J. Electrochem. Soc.* **156**, J112 (2009). <https://doi.org/10.1149/1.3095503>
18. C. He, K. Yang, L. Liu, Z. Si, Preparation and luminescence properties of $\text{BaWO}_4:\text{Yb}^{3+}/\text{Tm}^{3+}$ nano-crystal. *J. Rare Earths* **31**, 790–794 (2013). [https://doi.org/10.1016/S1002-0721\(12\)60359-7](https://doi.org/10.1016/S1002-0721(12)60359-7)
 19. L. Liu, K. Yang, X. Zhang, N. Qi, H. Li, Z. Zuo, Up-conversion luminescence properties of Yb^{3+} and Ho^{3+} co-doped $\text{Bi}_{3.84}\text{W}_{0.16}\text{O}_{6.24}$ powder synthesized by hydrothermal method. *J. Rare Earths* **30**, 1092–1095 (2012). [https://doi.org/10.1016/S1002-0721\(12\)60185-9](https://doi.org/10.1016/S1002-0721(12)60185-9)
 20. J.H. Chung, J.H. Ryu, S.W. Mhin, K.M. Kim, K.B. Shim, Controllable white upconversion luminescence in $\text{Ho}^{3+}/\text{Tm}^{3+}/\text{Yb}^{3+}$ co-doped CaMoO_4 . *J. Mater. Chem.* **22**, 3997–4002 (2012). <https://doi.org/10.1039/C2JM15332G>
 21. W. Gao, H. Zheng, Q. Han, E. He, R. Wang, Unusual upconversion emission from single $\text{NaYF}_4:\text{Yb}^{3+}/\text{Ho}^{3+}$ microrods under NIR excitation. *CrystEngComm* **16**, 6697–6706 (2014). <https://doi.org/10.1039/C4CE00627E>
 22. A. Salah, S.K. El-Mahy, O. El-sayed, I.K. Battisha, Up-conversion behaviors of nano-structure $\text{BaTi}_{0.9}\text{Sn}_{0.1}\text{O}_3$ activated by $\text{Er}^{3+}/\text{Yb}^{3+}$ ions. *Optik* **209**, 164571 (2020). <https://doi.org/10.1016/j.ijleo.2020.164571>
 23. K. Janani, S. Ramasubramanian, A.K. Soni, V.K. Rai, P. Thiagarajan, Luminescence properties of $\text{LiYF}_4:\text{Yb}^{3+}$, Er^{3+} phosphors: A study on influence of synthesis temperature and dopant concentration. *Optik* **169**, 147–155 (2018). <https://doi.org/10.1016/j.ijleo.2018.05.023>
 24. Q. Cheng, J. Sui, W. Cai, Enhanced upconversion emission in Yb^{3+} and Er^{3+} codoped NaGdF_4 nanocrystals by introducing Li^+ ions. *Nanoscale* **4**, 779–784 (2012). <https://doi.org/10.1039/C1NR11365H>
 25. C.S. Mao, X. Yang, L. Zhao, Simultaneous morphology control and upconversion fluorescence enhancement of $\text{NaYF}_4:\text{Yb}$, Er crystals through alkali ions doping. *Chem. Eng. J.* **229**, 429–435 (2013). <https://doi.org/10.1016/j.cej.2013.06.026>
 26. X. Chai, J. Li, X. Wang, Y. Li, X. Yao, Color-tunable upconversion photoluminescence and highly performed optical temperature sensing in $\text{Er}^{3+}/\text{Yb}^{3+}$ codoped ZnWO_4 . *Opt. Express* **24**, 22439–22447 (2016). <https://doi.org/10.1364/OE.24.022438>
 27. X.N. Chai, J. Li, Y. Zhang, X. Wang, Y. Li, Y. Xi, Bright dual-mode green emission and temperature sensing properties in $\text{Er}^{3+}/\text{Yb}^{3+}$ co-doped MgWO_4 phosphor. *RSC Adv.* **6**, 64072–64078 (2016). <https://doi.org/10.1039/C6RA09656E>
 28. B. Samanta, A.K. Dey, P. Bhaumik, S. Manna, A. Halder, D. Jana, K.K. Chattopadhyay, U.K. Ghorai, Controllable white light generation from novel $\text{BaWO}_4:\text{Yb}^{3+}/\text{Ho}^{3+}/\text{Tm}^{3+}$ nanophosphor by modulating sensitizer ion concentration. *J Mater Sci: Mater Electron* **30**, 1068–1075 (2019). <https://doi.org/10.1007/s10854-018-0375-4>
 29. A.K. Dey, B. Samanta, P. Bhaumik, S. Manna, A. Halder, T.K. Ghosh, T.K. Parya, U.K. Ghorai, Low-temperature synthesis of thermally stable $\text{BaWO}_4:\text{Yb}^{3+}:\text{Ho}^{3+}$ nanophosphors: Tuning visible emission by controlling activator ion concentration. *J. Lumin.* **211**, 251–257 (2019). <https://doi.org/10.1016/j.jlumin.2019.03.020>
 30. R.D. Shannon, Revised effective ionic radii and systemic studies of interatomic distances in halides and chalcogenides. *Acta Cryst. A* **32**, 751–767 (1976). <https://doi.org/10.1107/S0567739476001551>
 31. L. Xu, J. Liu, L. Pei, Y. Xu, Z. Xia, Enhanced up-conversion luminescence and optical temperature sensing in graphitic C_3N_4 quantum dots grafted with $\text{BaWO}_4:\text{Yb}^{3+}$, Er^{3+} phosphors. *J. Mater. Chem. C* **7**, 6112–6119 (2013). <https://doi.org/10.1039/C9TC01351B>
 32. N. Dhananjaya, H. Nagabhushana, B.M. Nagabhushana, B. Rudraswamy, Enhanced photoluminescence of $\text{Gd}_2\text{O}_3:\text{Eu}^{3+}$ nanophosphors with alkali ($\text{M} = \text{Li}^+$, Na^+ , K^+) metal ion codoping. *Acta Part A Mol. Biomol. Spectrosc.* **86**, 8–14 (2012). <https://doi.org/10.1016/j.saa.2011.05.072>
 33. B.P. Singh, A.K. Parchur, R.S. Ningthoujam, P.V. Ramakrishna, S. Singh, P. Singh, S.B. Raib, R. Maalej, (2014) Enhanced up-conversion and temperature-sensing behaviour of Er^{3+} and Yb^{3+} co-doped $\text{Y}_2\text{Ti}_2\text{O}_7$ by incorporation of Li^+ ions. *Phys. Chem. Chem. Phys.* **16**, 22665–22676 (2014). <https://doi.org/10.1039/C4CP02949F>
 34. R. Chakraborty, A. Maiti, U.K. Ghorai, A.J. Pal, Defect passivation of Mn^{2+} -doped CsPbCl_3 perovskite nanocrystals as probed by scanning tunneling spectroscopy: Toward boosting emission efficiencies. *ACS Appl. Nano Mater* (2021). <https://doi.org/10.1021/acsanm.1c01623>

Publisher's Note Springer Nature remains neutral with regard to jurisdictional claims in published maps and institutional affiliations.